electronics

MDPI

Article

A Method for Fingerprint Edge Enhancement Based on Radial Hilbert Transform

Baiyang Wu [1,2], Shuo Zhang [1], Weinan Gao [1,*], Yong Bi [1] and Xiaosong Hu [3]

[1] Applied Laser Research Center, Technical Institute of Physics and Chemistry, Chinese Academy of Sciences, Beijing 100190, China; wubaiyang22@mails.ucas.ac.cn (B.W.); zhangshuo@mail.ipc.ac.cn (S.Z.); biyong@mail.ipc.ac.cn (Y.B.)
[2] University of Chinese Academy of Sciences, Beijing 100049, China
[3] Suzhou Xiaosong Technology Development Co., Ltd., Suzhou 215000, China; xiaosonglasearcher@outlook.com
* Correspondence: wngao@mail.ipc.ac.cn

Abstract: Fingerprints play a significant role in various fields due to their uniqueness. In order to effectively utilize fingerprint information, it is necessary to enhance image quality. This paper introduces a method based on Radial Hilbert transform (RHLT), which simulates the vortex filter using the point spread function (PSF) of spiral phase plate (SPP) with a topological charge $l = 1$, for fingerprint edge enhancement. The experimental results show that the processed fingerprint image has more distinct edges, with an increase in information entropy and average gradient. Unlike classical edge detection operators, the fingerprint edge image obtained by the RHLT method exhibits a lower mean square error (MSE) and a higher peak signal-to-noise ratio ($PSNR$). This indicates that the RHLT method provides more accurate edge detection and demonstrates higher noise-resistance capabilities. Due to its ability to highlight edge information while preserving more original features, this method has great application potential in fingerprint image processing.

Keywords: fingerprint; Radial Hilbert transform; edge enhancement; edge detection

check for updates

Citation: Wu, B.; Zhang, S.; Gao, W.; Bi, Y.; Hu, X. A Method for Fingerprint Edge Enhancement Based on Radial Hilbert Transform. *Electronics* **2024**, *13*, 3886. https://doi.org/10.3390/electronics13193886

Academic Editor: Valentina E. Balas

Received: 7 August 2024
Revised: 3 September 2024
Accepted: 9 September 2024
Published: 30 September 2024

Copyright: © 2024 by the authors. Licensee MDPI, Basel, Switzerland. This article is an open access article distributed under the terms and conditions of the Creative Commons Attribution (CC BY) license (https://creativecommons.org/licenses/by/4.0/).

1. Introduction

Fingerprints, composed of many ridges and valleys, are different for each individual and remain unchanged throughout life. Thanks to its uniqueness and permanence, fingerprints are crucial for identity verification, criminal investigations, security identification and other areas [1–3]. Commonly, a fingerprint recognition system includes four stages: acquisition, pre-processing, feature extraction and matching. Since the contours and edges of fingerprint images contain essential information, edge detection is a fundamental method useful in image pre-processing [4,5]. This technique highlights the characteristics of fingerprint shapes, allowing for the identification of fingerprint sources based on features such as gaps, directions, and breakpoints. Then, enhancing fingerprints can make the images clearer and is beneficial for ensuring the reliability of minutiae, facilitating subsequent feature extraction and matching [6,7].

The classical edge detection algorithm identifies the edges of fingerprint images using gradient operators, which analyze the changes in gray values within the neighborhood [8–10]. This method involves spatial domain image processing. In an image, edges represent regions of rapid change, while non-edge areas indicate slower changes. The technique directly applies differentiation operations to the image pixels. The common edge detection operators include the Roberts operator, Prewitt operator, Sobel operator, Canny operator, LoG operator and so on. Among them, Roberts, Prewitt, Sobel and Canny use first-order derivatives, which operate at points of larger gradient values, while the LoG uses second-order derivatives, which operate at points where zero-crossing occurs. These operators, acting as convolution kernels, can be seen as two templates with specific sizes and element

values in the x and y directions, and are used to convolve each point in the image, thereby obtaining edge information. They have a similar principle of calculating gradient values by convolving the image with a small mask. However, gradient operators are sensitive to noise, and the resulting edge curves may be discontinuous or incomplete.

In fact, there is another method useful in edge detection and enhancement, which is Hilbert transform (HLT); this uses Fourier transform-based spatial filtering to process images in the frequency domain. Different frequency components convey different information: low-frequency components represent the smooth and non-edge regions of the image, while high-frequency components represent the details and edge information. By filtering the frequency spectrum of the incident light field or modifying the frequency components of the input image, specific components can be selectively passed or removed to achieve the desired effect. In 1966, Bracewell et al. proposed a spatial filtering operation based on HLT and fractional HLT to achieve one-dimensional (1D) edge enhancement [11]. In 1992, Khonina et al. used photolithography to manufacture a spiral phase plate (SPP) and implemented it as a phase filter for edge detection of a aperture diaphragm [12]. In 2000, Davis et al. proposed a method to implement radial Hilbert transform (RHLT) by using a liquid crystal spatial light modulator to load SPP onto the spectrum plane of a 4f optical system; this is also known as vortex filtering and can achieve isotropic edge enhancement [13]. Subsequently, the effectiveness of this spatial filtering method was gradually recognized, leading to extensive research and application. In image processing, the two-dimensional (2D) HLT and the generalized RHLT have been used in optical information processing to realize image edge detection [14,15]. In experiments, vector vortex filters have been proposed to achieve selective edge enhancement [16–18]. Additionally, nonlinear vortex filtering was utilized for mid-infrared single-photon edge-enhanced imaging, expanding the operational wavelength range [19]. As vortex filtering technology continues to advance, it has found numerous applications in various fields, such as biomedical imaging and quantum imaging [20–23]. Nevertheless, few people have applied the RHLT method to biometric feature enhancement. In 2012, Y. J. Morales et al. used RHLT as a tool for edge detection in fingerprint images captured by biometric sensors. However, since only a simple consideration of frequency transformation was made, the resulting images still require further improvement [24]. Given that each region of a fingerprint image contains different directional fields, and that RHLT using SPP as a scalar vortex filter is independent of the local orientation of the image, we consider processing the image by analyzing the optical system's point spread function (PSF) and using a simulation method that more accurately reflects real filtering conditions. Meanwhile, beyond processing electronically scanned fingerprints from biometric sensors, we intend to apply the RHLT method to latent fingerprints at crime scenes, extending into the field of criminal investigation to address challenges such as difficult evidence detection and unclear features. In this paper, a method of fingerprint edge detection and enhancement based on RHLT is proposed. We analyze the PSF of an SPP and use it as a convolution kernel to perform RHLT on input fingerprint images, which significantly improves the image quality. Then, we compared RHLT with classical edge detection operators and confirmed that the edge curves obtained by RHLT are closer to the original fingerprint morphology, showing better noise resistance.

2. Theory and Method

2.1. Principle of Radial Hilbert Transform

The 1D HLT is defined as

$$\tilde{g}(x,y) = g(x,y) * \frac{1}{\pi x} \tag{1}$$

where $g(x,y)$ is an input image and $\tilde{g}(x)$ is an output image. $1/(\pi x)$ is the impulse response function of transform system; its Fourier transform form $H(\mu)$ is:

$$H(u) = \begin{cases} \exp(i\frac{\pi}{2}), u > 0 \\ 0, u = 0 \\ \exp(-i\frac{\pi}{2}), u < 0 \end{cases} \quad (2)$$

It is apparent that through this spatial filtering operation, the positive frequency shifts by $\pi/2$ while the negative frequency shifts by $-\pi/2$, and a phase difference of π is generated between them. The interference effect from the phase difference amplifies the high-frequency components in the spatial domain, enhancing edge contrast and sharpening the image in a specific direction. Its corresponding 1D HLT filter is shown in Figure 1a. Moreover, to extend this transformation to a two-dimensional plane, the simplest method is to combine two 1D HLT along the x and y directions to form a 2D HLT; the expression is

$$\tilde{g}(x,y) = g(x,y) * \frac{1}{\pi x} * \frac{1}{\pi y} \quad (3)$$

Furthermore, to extend HLT to all directions, a method using vortex filter for RHLT has been proposed. The basic idea is to introduce a spiral phase in the frequency plane, with the phase continuously varying and a phase difference of π along any radial direction. Each straight line passing through the singularity corresponds to a 1D HLT filter. The SPP, a representative type of vortex element, is a phase-only diffractive optical element with optical thickness proportional to the rotation azimuth ϕ. Its transmittance function can be expressed as

$$H(\rho,\phi) = circ(\frac{\rho}{R})exp(il\phi) \quad (4)$$

where (ρ,ϕ) represents polar coordinates in the frequency domain; R is the aperture of SPP; l is the topological charge. The RHLT filter is shown in Figure 1b. Applying the Fourier transform to Equation (4) converts the frequency domain function into the spatial domain, resulting in the PSF of the SPP. To achieve isotropic edge enhancement, the case of $l = 1$ is used, and the PSF can be approximated as

$$h(r,\theta) = -\frac{2\pi}{\lambda f}\exp(i\theta)\int_0^R J_1\left(\frac{2\pi\rho r}{\lambda f}\right)\rho d\rho = -i\frac{\pi R}{2r}[J_1(x)H_0(x) - J_0(x)H_1(x)]\exp(i\theta) \quad (5)$$

where $x = 2\pi Rr/\lambda f$; λ is the wavelength of the incident light wave; f is the focal length of the Fourier transform lens. J_0 and J_1 are the zeroth-order and first-order Bessel functions of the first kind, respectively; H_0 and H_1 are the zeroth-order and first-order Struve functions, respectively. It is important to note that the topological charge represents the number of 2π phase shifts around the center. As topological charge increases, higher-order vortex filtering causes more intense frequency rotation, leading to more pronounced distortions. This may emphasize features like sharp corners and curved edges but can hinder balanced edge enhancement.

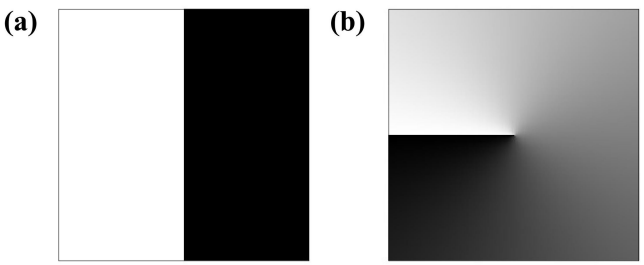


Figure 1. Phase distribution: (**a**) 1D HLT; (**b**) RHLT for $l = 1$. Gray levels represent different phase values.

The $h(r,\theta)$ is used as the convolution kernel and is convolved with the input image to obtain the output image after RHLT:

$$\tilde{g}(x,y) = g(x,y) * h(r,\theta) \tag{6}$$

When performing a convolution calculation, the PSF assigns weights to each point in the input image and then integrates over the entire region. The uniform regions of the image correspond to slowly varying low-frequency information, where the PSF induces a phase shift between any adjacent points, causing destructive interference that results in a dark field. Conversely, the edges and minutiae of the image correspond to high-frequency information. The destructive interference process is imperfect, leading to the enhancement of edges. It is worth noting that the PSF of SPP describes the filter's effect in the spatial domain. By directly convolving the image with the PSF, the filtering process can be accomplished in a single convolution operation, avoiding the need for two Fourier transforms and thereby reducing computational complexity.

2.2. Simulate the PSF of SPP

We calculate this process in MATLAB 2023. Suppose there is a $4f$ optical system, lens 1 takes the Fourier transform of the input image, and lens 2 takes the inverse Fourier transform. SPP is placed in the Fourier plane for vortex filtering, and the output image is the RHLT of the input image. The specific parameters are set as follows: the radius of the SPP is 4.5 mm, the incident light wavelength is 532 nm, and the focal length of the Fourier transform lens is 100 mm.

The PSF of SPP is simulated using Equation (5), and the resulting radial distribution curve is shown in Figure 2. It can be seen that the PSF consists of a primary maximum and several secondary maxima. Convolution of the input image with the primary maximum highlights areas where gray values change in any direction, achieving isotropic edge enhancement. Convolution with the secondary maxima results in some diffraction noise distributed around the edge-enhanced areas, creating a relief effect [25].

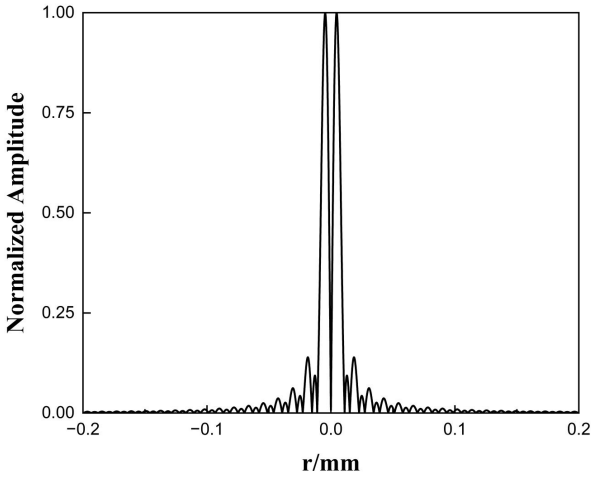


Figure 2. Radial distribution curve of SPP.

3. Experiment and Analysis

In our work, the application of RHLT is targeted at latent fingerprints and electronic fingerprint images. Latent fingerprints are used to discuss the enhancement effects of RHLT, while electronic fingerprints are used to compare the differences between RHLT and other edge detection operators. As mentioned previously, there are indeed some differences between these two types of fingerprints: latent fingerprints are those that are difficult to detect with the naked eye and are extracted from surfaces at crime scenes using special techniques. This method is constrained by the conditions at the scene and the state of the surface, so the fingerprints obtained may be blurry or incomplete, thus requiring image processing to enhance their features. On the other hand, electronic fingerprints are directly captured using biometric sensors, recording fingerprint details through electrical signals or

optical technologies. This method typically captures high-resolution fingerprint images, making it suitable for comparing the edge processing effects of different algorithms.

In Section 3, the edge enhancement effect of RHLT on latent fingerprints is initially discussed. The steps are as follows:

1. Fingerprint image acquisition: Recording sweat fingerprints left on porous surfaces using photoluminescence photography.
2. Fingerprint image pre-processing: Converting the original images to grayscale and reducing noise with Gaussian filtering.
3. Fingerprint image edge enhancement: Applying RHLT to the pre-processed grayscale images and enhancing the images through linear grayscale stretch. The transformed and enhanced fingerprint images are then output.

3.1. Fingerprint Image Acquisition

First, a laser was used to excite the fluorescence of latent fingerprints treated with chemical reagents in the experiment. The schematic diagram of the experiment is shown in Figure 3a. To prepare fingerprint samples, sweaty fingers are pressed on the surface of the paper, then an amino acid-sensitive reagent is sprayed on it. The indanedione in the reagent reacts with the amino acids in sweat to produce an intermediate product that fluoresces under specific illuminating conditions [26]. Figure 3b shows the photoluminescence spectrum of the fluorescent product. Fluorescence is a type of photoluminescence phenomenon; when molecules or atoms of a substance absorb photons that meet a certain energy difference, electrons are excited to higher energy levels. These excited electrons quickly return to their ground state, emitting new photons in the process. The emitted photons typically have a longer wavelength than the absorbed ones, known as the Stokes shift. It can be seen that under excitation with 532 nm green light, the emitted fluorescence spectrum ranges from 550 to 650 nm.

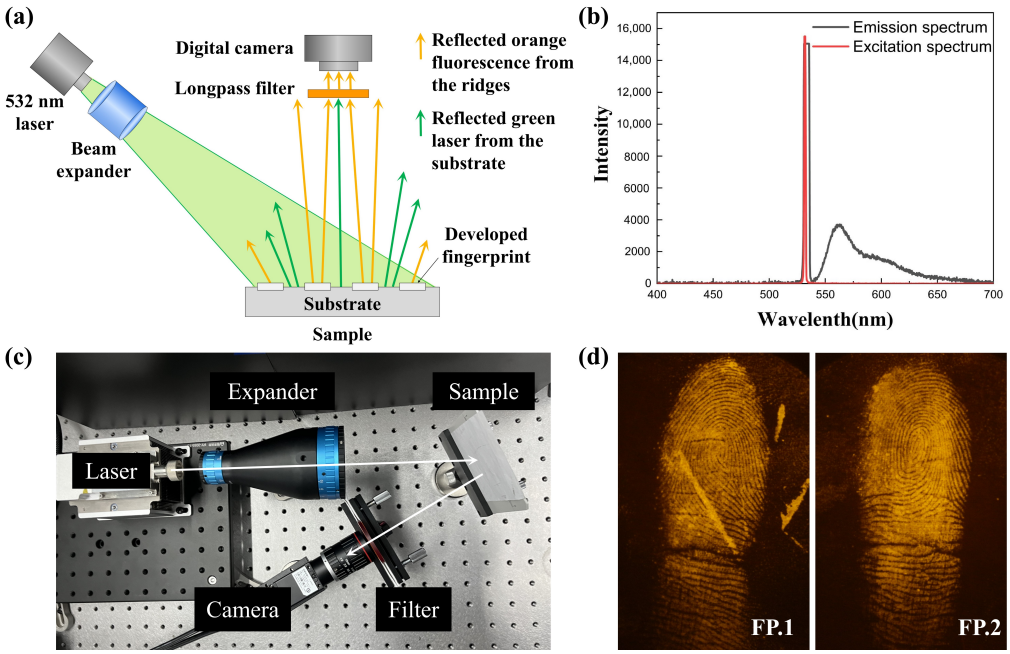


Figure 3. (**a**) Schematic diagram of the experiment for fingerprint acquisition; (**b**) photoluminescence spectra of a latent fingerprint treated with indanedione; (**c**) optical layout of the experimental setup; (**d**) the original fingerprint images of FP. 1 and FP. 2.

The optical layout of the experimental setup is shown in Figure 3c. At the emitting end, a laser operating at a wavelength of 532 nm is used to illuminate the sample surface after passing through a beam expander, exciting the fluorescence of the fingerprint sample. At the receiving end, a long-pass filter is used to block the short-wavelength excitation

light, allowing the longer-wavelength fluorescence to pass through. Then, images were captured and recorded with a digital camera. When exposed to green excitation light, latent fingerprints emit orange-yellow fluorescence. The original images of FP. 1 and FP. 2 are shown in Figure 3d. There is an uneven distribution of amino acid components in sweat residue on paper; the fluorescence intensity of stimulated fingerprints varies accordingly. In areas with densely packed and wider ridge lines, the indanedione complex products are more concentrated, leading to higher fluorescence intensity under laser illumination.

3.2. Fingerprint Image Pre-Processing

Before implementing RHLT, the original fingerprint images need to be pre-processed. Firstly, because different regions of fingerprint images exhibit varying levels of light intensity reflecting changes in fluorescence intensity, we convert the color image to grayscale. This translation assigns fluorescence intensity to grayscale values, facilitating subsequent image processing.

Secondly, because the long-pass filter cannot completely eliminate irrelevant stray light, there is background noise interference in grayscale images, which needs to be denoised. Gaussian filtering is a linear smoothing image processing technique suitable for reducing background noise while preserving edge features and maintaining image details. Its function form is

$$G(x,y) = \frac{1}{2\pi\sigma^2} e^{-\frac{x^2+y^2}{2\sigma^2}} \tag{7}$$

where σ is the standard deviation, which we assume to be 1 to avoid excessive blurring of image details. The preprocessed fingerprint images of FP. 1 and FP. 2 are shown in Figure 4a and 4c, respectively.

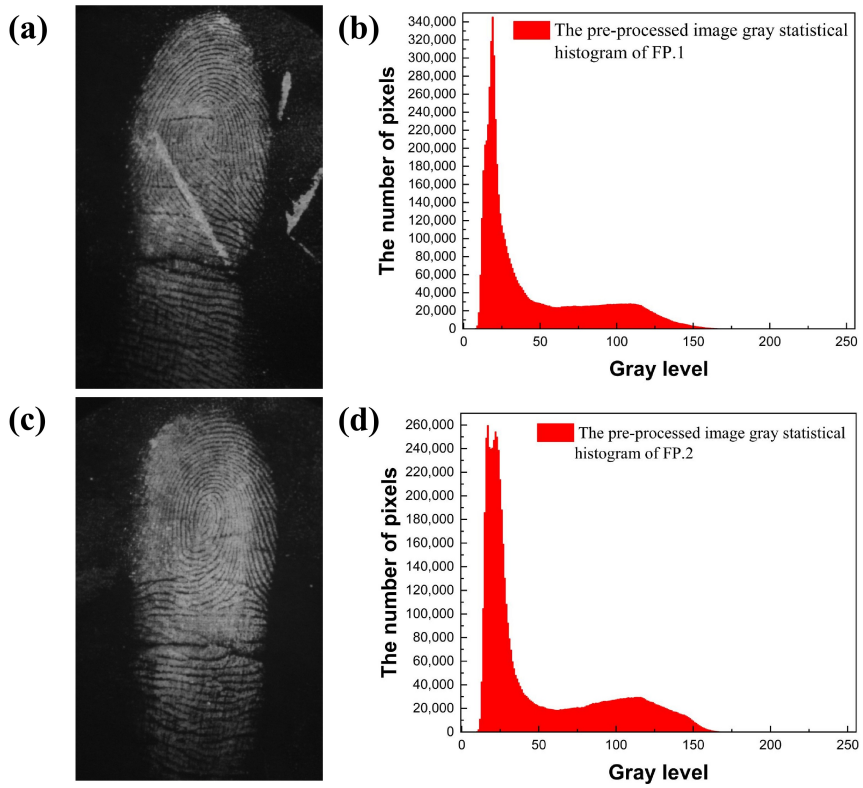


Figure 4. The pre-processed grayscale images and their gray statistical histogram: (**a**,**b**) for FP. 1; (**c**,**d**) for FP. 2.

The number of pixels at each grayscale level is represented by grayscale histograms, which are displayed in Figure 4b,d, respectively. It can be observed that the histograms exhibit a single peak and are primarily concentrated on the left side. This is due to the long-

pass filter blocking most of the light and the relatively weak fluorescence intensity, resulting in an overall low image brightness. Pixels with grayscale values below 50 correspond to the dark background of the image, while those with values above 50 represent the fluorescent regions of the fingerprint.

3.3. Fingerprint Image Edge Enhancement

Next, RHLT is applied to the pre-processed images, resulting in the transformed images shown in Figure 5a,c. It can be seen that the high-frequency details of fingerprint ridges are emphasized, while overexposed or slowly changing low-frequency areas darken. All edge features of the original image are preserved, presenting the fingerprint overall with a relief effect. The grayscale histograms of transformed images of FP. 1 and FP. 2 are shown in Figure 5b,d, respectively. The grayscale values near the fingerprint ridges in the dark background increase due to the edge enhancement effect, thereby enhancing the fluorescent regions.

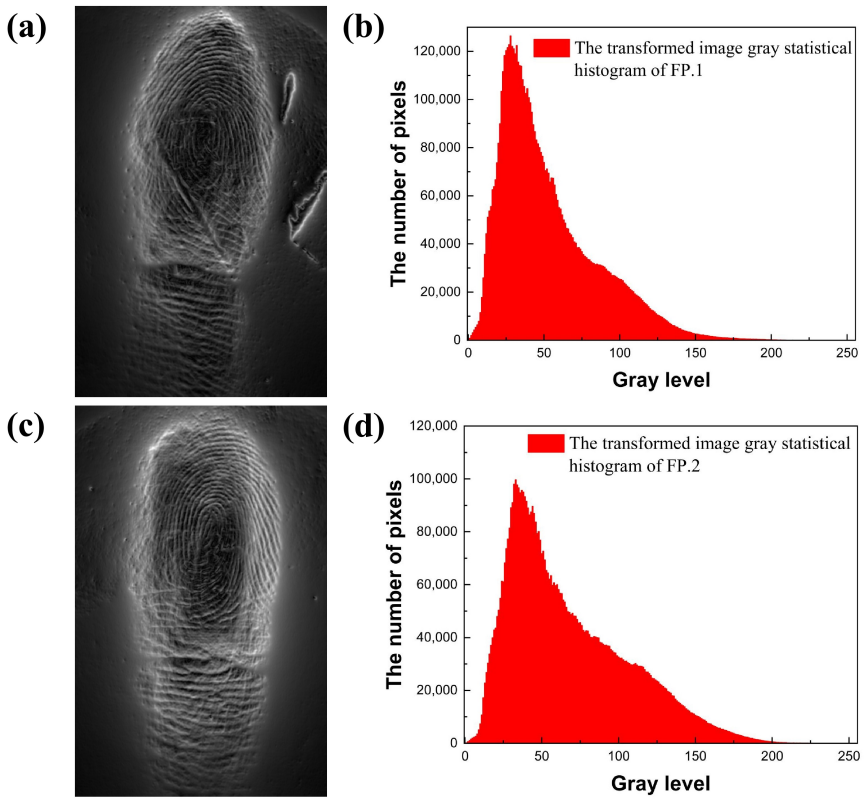


Figure 5. The transformed images after RHLT and their gray statistical histogram: (**a**,**b**) for FP. 1; (**c**,**d**) for FP. 2.

To further improve the visual effect of the images, a linear grayscale stretch was applied to each pixel of the transformed images. This technique adjusts the grayscale values within the image to span the full range, enhancing contrast and making finer details more visible. If we assume that the transformed image $f(i,j)$ has a grayscale range of $[a,b]$, and the enhanced image $g(i,j)$ has a grayscale range of $[c,d]$, then there is a relationship between them:

$$g(i,j) = c + \frac{d-c}{b-a}[f(i,j) - a] \tag{8}$$

The enhanced images after grayscale stretch are shown in Figure 6a,c, and their corresponding grayscale histograms are shown in Figure 6b,d. This indicates that the linear grayscale stretch enhances the overall brightness of the images and separates certain pixel levels, making features more distinct.

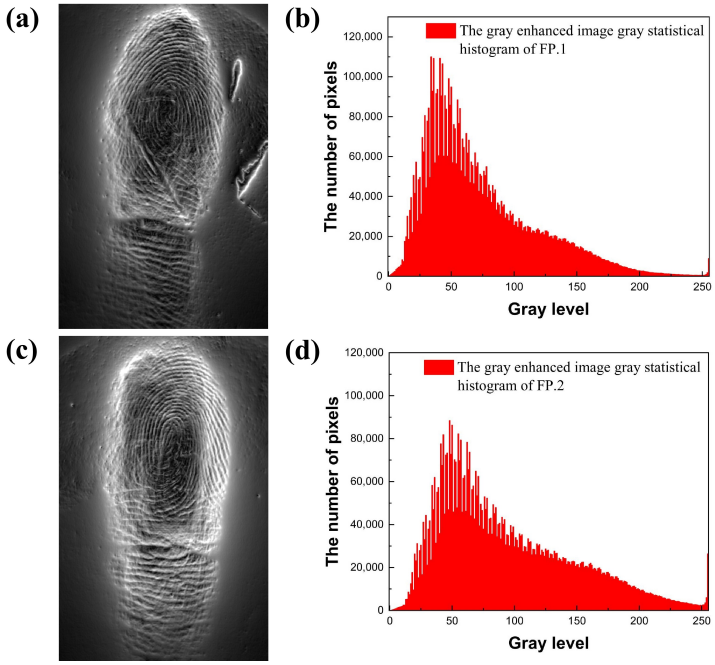


Figure 6. The gray, enhanced images and their gray statistical histogram: (**a**,**b**) for FP. 1; (**c**,**d**) for FP. 2.

If we compare grayscale images in Figure 4 with enhanced images in Figure 6, and evaluate image quality using two metrics, information entropy H and average gradient $\bar{G}$, which are defined as follows, then

$$H = -\sum_{i=0}^{255} P(i) log_2 P(i) \tag{9}$$

and

$$\bar{G} = \frac{1}{M \times N} \sum_{i=1}^{M} \sum_{j=1}^{N} \sqrt{G_x(i,j)^2 + G_y(i,j)^2} \tag{10}$$

where $P(i)$ is the probability of grayscale level i. M and N are the height and width of the image, respectively; $G_x(i,j)$ and $G_y(i,j)$ are the horizontal and vertical gradients at position (i,j). The information entropy quantifies the amount of feature information present in an image, with a higher entropy indicating greater richness of information. The average gradient measures the image's minutiae and edges, with higher average gradient values indicating that the image has more details and clear edges. From Table 1, it can be seen that the information entropy and average gradient of the images have been improved after RHLT and enhancement. This indicates that the RHLT method effectively highlights fingerprint features and enhances edges, resulting in higher image quality, which is useful in criminal investigations. Furthermore, the RHLT method is enhanced based on the frequency information of the original image, which can avoid the introduction of forged information.

Table 1. Comparison of information entropy and mean gradient between gray image and enhanced image.

		Information Entropy	Mean Gradient
FP. 1	Grayscale image	6.3736	12.5161
	Enhanced image	7.2414	16.8476
FP. 2	Grayscale image	6.3946	11.7558
	Enhanced image	7.5449	17.5258

4. Comparison and Discussion

In Section 4, the RHLT-based algorithm is compared with edge detection operators such as Roberts, Sobel, Prewitt, Canny, and LoG, using electronic fingerprints scanned and recorded by biometric sensors from the public domain. Initially, two high-quality fingerprint images, as shown in Figure 7, with pixel dimensions of 1992 × 2788 pixels and 1386 × 2080 pixels, respectively, are used to compare the edge detection performance of different algorithms.

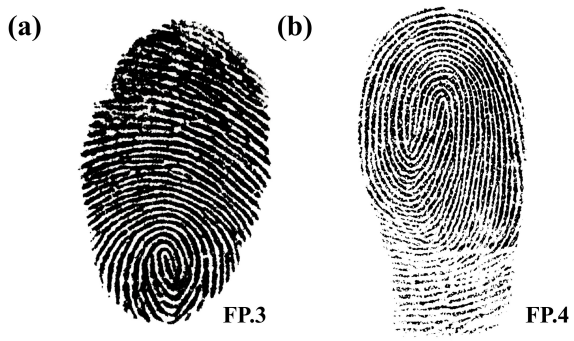


Figure 7. High-quality fingerprint images from public domain: (**a**) FP. 3; (**b**) FP. 4.

The edge detection results of FP. 3 and FP. 4 are shown in Figure 8 and Figure 9, respectively. The figures show that classical edge detection operators perform similarly in fingerprint edge detection, with slight differences in some details. The resulting images are binarized through a thresholding process. In contrast, RHLT processes the frequency information of the input image, enhancing high-frequency details and suppressing low-frequency background, resulting in strengthened fingerprint edges.

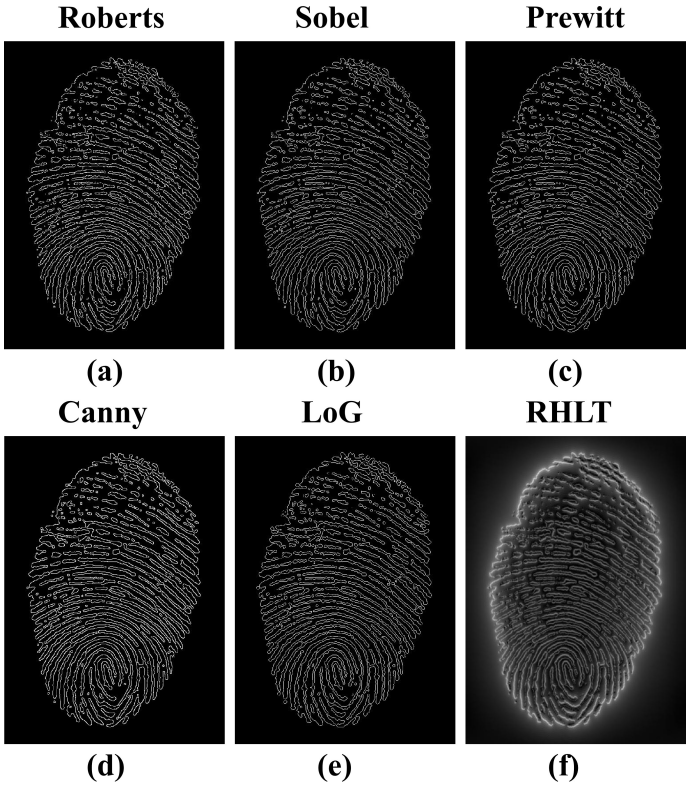


Figure 8. Edge detection for FP. 3: (**a**) Roberts; (**b**) Sobel; (**c**) Prewitt; (**d**) Canny; (**e**) LoG; (**f**) RHLT.

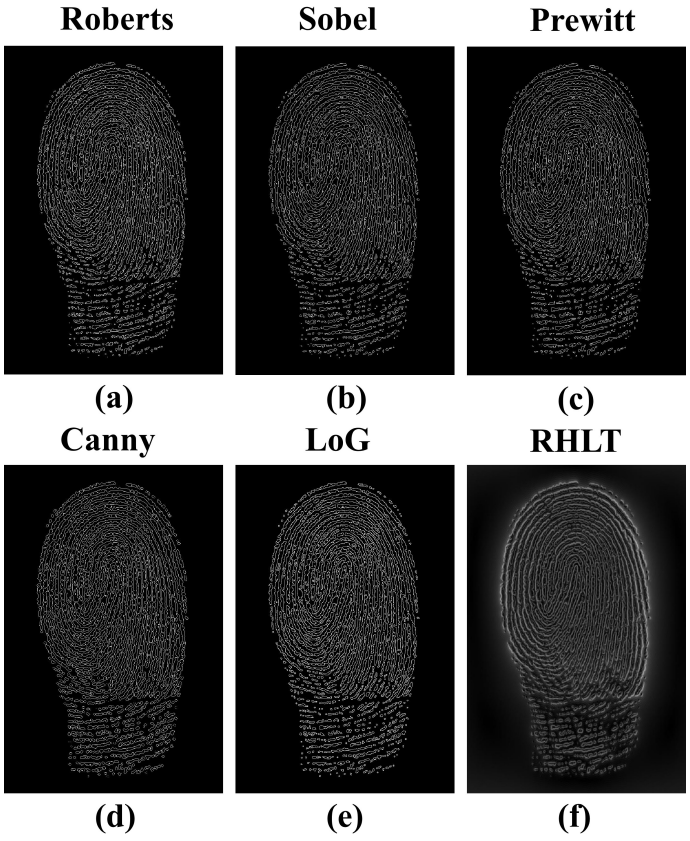


Figure 9. Edge detection for FP. 4: (**a**) Roberts; (**b**) Sobel; (**c**) Prewitt; (**d**) Canny; (**e**) LoG; (**f**) RHLT.

These two parameters, mean square error (MSE) and peak signal-to-noise ratio ($PSNR$), are used to compare the image quality of different algorithms:

$$MSE = \frac{1}{M \times N} \sum_{i=1}^{M} \sum_{j=1}^{N} [\tilde{g}(i,j) - g(i,j)] \tag{11}$$

and

$$PSNR = 10log_{10}(\frac{Max^2}{MSE}) \tag{12}$$

where $\tilde{g}(i,j)$ is the processed edge image, $g(i,j)$ is the original reference image, and Max is the maximum possible value of the original image. For an 8-bit grayscale image, the value of Max is typically 255. MSE measures the average squared differences between the edge image and original image. A higher MSE indicates larger discrepancies and higher error in edge detection, while a lower MSE indicates more accurate detection. $PSNR$ is the ratio of peak signal power-to-average noise power. A lower $PSNR$ means more noise and distortion, whereas a higher $PSNR$ means the processed image is more similar to the original with less noise. Therefore, a lower MSE and a higher $PSNR$ are preferable, indicating better correlation between the processed and original images and more accurate fingerprint edge detection.

The edge-detected images from Figures 8 and 9 were compared with the original images of FP. 3 and FP. 4 in Figure 7, respectively. The MSE and PSNR values were calculated, and the results obtained from different algorithms are shown in Table 2. The experimental results indicate that the Roberts, Sobel and Prewitt operators yield similar effects in fingerprint edge detection and are capable of handling detail-rich fingerprint images but are susceptible to noise interference. The Canny operator can detect the main edges of fingerprints; however, its smoothing effect may occasionally lead to an oversight of some edge details. In contrast, the LoG operator effectively reduces noise, accurately identifies

fingerprint edges, and produces higher-quality images. It is particularly noteworthy that the algorithm based on RHLT achieves lower *MSE* and higher *PSNR*, indicating detection of more abundant edge details and demonstrating higher image quality. The proposed algorithm extracts smoother, more continuous edges that are closer to the true edges in the original image, meeting visual and quality requirements for practical image applications.

Table 2. Comparison of *MSE* and *PSNR* of fingerprint images using different edge detection operators and RHLT method.

		Roberts	Sobel	Prewitt	Canny	LoG	RHLT
FP. 3	MSE	37577	37518	37521	38159	36968	27225
	PSNR	2.3816	2.3884	2.3880	2.3148	2.4526	3.7812
FP. 4	MSE	50862	50881	50850	50729	47836	41644
	PSNR	1.0669	1.0652	1.0679	1.0782	1.3333	1.9353

To further demonstrate the method's generality, algorithm comparisons were implemented on the DB1 subcategory of the Fingerprint Verification Competition (FVC) 2004 fingerprint database. This subcategory contains 80 fingerprint images from 10 volunteers, with each volunteer providing 8 images of varying quality from the same finger. The size of each image is 640 × 480 pixels. Different algorithms, including RHLT, Roberts, Sobel, Prewitt, Canny and LoG, were used for edge detection on each image, followed by calculating the MSE and PSNR values in comparison to the corresponding original images. The eight images from the same finger were then averaged, resulting in 10 sets of averages. As shown in Figure 10a,b, the average MSE and PSNR values for these images are plotted, with the horizontal axis representing the sequence numbers of the 10 fingerprint sets. The curves in different colors represent the values obtained from different algorithms. The curves for different algorithms exhibit similar trends, indicating that they show comparable stability in processing different images. Among the gradient operator algorithms, the curves for the Roberts, Sobel, and Prewitt algorithms almost overlap, indicating similar processing capabilities. The LoG algorithm has the second-lowest MSE and the second-highest PSNR, suggesting it performs the best among the gradient operators, with the Canny algorithm following closely. Notably, the RHLT algorithm has the lowest MSE and the highest PSNR, suggesting it offers better noise resistance.

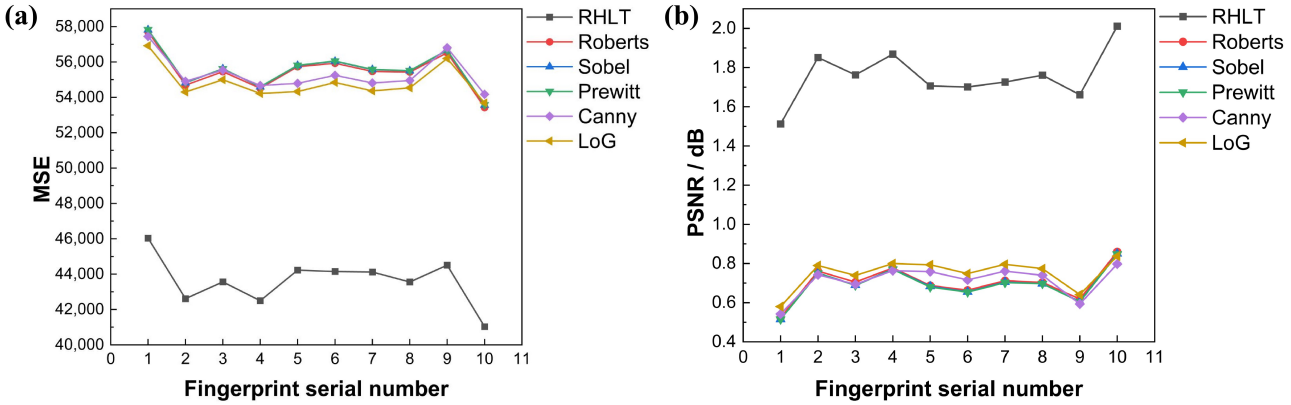


Figure 10. Comparison of values processed by different algorithms: (**a**) MSE; (**b**) PSNR.

5. Conclusions

In this paper, an edge enhancement method based on RHLT is proposed to process fingerprint images. We collected latent fingerprint images in the experiment and applied the proposed RHLT algorithm to them, effectively increasing information entropy and the average gradient of images. This demonstrates that the method is useful and feasible for

improving image quality. Subsequently, electronic fingerprint images of different sizes from public datasets were used to compare the edge detection performance of the RHLT method with classical gradient operators. The results indicate that, compared to other edge detection operators, RHLT shows lower MSE and higher $PSNR$, avoiding false edges and ensuring accurate detection. Furthermore, it can also be observed from the results that due to the presence of secondary peaks in the PSF, the processed image exhibits some relief effects. If this phenomenon is undesirable, it can be mitigated by suppressing the sidelobes. This algorithm provides an approach for fingerprint image processing and edge enhancement, and it also has great potential for application to other targets.

Author Contributions: Conceptualization, B.W. and W.G.; methodology, B.W. and S.Z.; software, B.W.; validation, Y.B. and W.G.; formal analysis, B.W.; investigation, B.W. and S.Z.; resources, Y.B. and X.H.; data curation, B.W. and W.G.; writing—original draft preparation, B.W.; writing—review and editing, S.Z. and W.G.; visualization, B.W.; supervision, W.G. and S.Z.; project administration, W.G., Y.B. and X.H.; funding acquisition, Y.B. All authors have read and agreed to the published version of the manuscript.

Funding: This research received no external funding.

Data Availability Statement: The data presented in this study are available on request from the corresponding author.

Conflicts of Interest: All authors are collaborators and are not employed by any commercial companies. The authors declare no conflicts of interest.

Abbreviations

The following abbreviations are used in this manuscript:

HLT	Hilbert transform
RHLT	Radial Hilbert transform
SPP	Spiral phase plate
PSF	Point spread function
FP	Fingerprint
MSE	Mean square error
PSNR	Peak signal-to-noise ratio

References

1. Win, K.N.; Li, K.; Chen, J.; Viger, P.F.; Li, K. Fingerprint classification and identification algorithms for criminal investigation: A survey. *Future Gener. Comput. Syst.* **2020**, *110*, 758–771. [CrossRef]
2. Lennard, C. Fingerprint detection: Current capabilities. *Aust. J. Forensic Sci.* **2007**, *39*, 55–71. [CrossRef]
3. Ali, M.M.; Mahale, V.H.; Yannawar, P.; Gaikwad, A. Overview of fingerprint recognition system. In Proceedings of the 2016 IEEE International Conference on Electrical, Electronics, and Optimization Techniques (ICEEOT), Chennai, India, 3–5 March 2016; pp. 1334–1338.
4. Weina, Z.; Jun, H.; Xiaoyang, Z.; Weiwei, Y. Fingerprint verification based on wavelet and edge detection. In Proceedings of the 2009 9th IEEE International Conference on Electronic Measurement & Instruments, Beijing, China, 16–19 August 2009; pp. 3-1001–3-1004.
5. Chanklan, R.; Chaiyakhan, K.; Hirunyawanakul, A.; Kerdprasop, K.; Kerdprasop, N. Fingerprint recognition with edge detection and dimensionality reduction techniques. In Proceedings of the 3rd International Conference on Industrial Application Engineering, Tokyo, Japan, 14–15 December 2015.
6. Hong, L.; Jian, A. Fingerprint enhancement. In Proceedings of the Third IEEE Workshop on Applications of Computer Vision. WACV'96, Sarasota, FL, USA, 2–4 December 1996; pp. 202–207.
7. Karo, N.N.B.; Sari, A.Y.; Aziza, N.; Putra, H.K. The enhancement of fingerprint images using gabor filter. In Proceedings of the Journal of Physics: Conference Series, Palembang, Indonesia, 26–27 November 2018; Volume 1196, p. 012045.
8. Cui, W.; Wu, G.; Hua, R.; Yang, H. The research of edge detection algorithm for Fingerprint images. In Proceedings of the 2008 IEEE World Automation Congress, Hawaii, HI, USA, 28 September–2 October 2008; pp. 1–5.
9. Ali, M.M.; Yannawar, P.; Gaikwad, A. Study of edge detection methods based on palmprint lines. In Proceedings of the 2016 IEEE International Conference on Electrical, Electronics, and Optimization Techniques (ICEEOT), Chennai, India, 3–5 March 2016; pp. 1344–1350.

10. Srujana, P.; Priyanka, J.; Patnaikuni, V.S.; Vejendla, N. Edge Detection with different Parameters in Digital Image Processing using GUI. In Proceedings of the 2021 5th IEEE International Conference on Computing Methodologies and Communication (ICCMC), Erode, India, 8–10 April 2021; pp. 795–802.
11. Bracewell, R.; Kahn, P.B. The Fourier transform and its applications. *Am. J. Phys.* **1966**, *34*, 712–712. [CrossRef]
12. Khonina, S.; Kotlyar, V.; Shinkaryev, M.; Soifer, V.; Uspleniev, G. The phase rotor filter. *J. Mod. Opt.* **1992**, *39*, 1147–1154. [CrossRef]
13. Davis, J.A.; McNamara, D.E.; Cottrell, D.M.; Campos, J. Image processing with the radial Hilbert transform: Theory and experiments. *Opt. Lett.* **2000**, *25*, 99–101. [CrossRef] [PubMed]
14. Pei, S.C.; Ding, J.J. The generalized radial Hilbert transform and its applications to 2D edge detection (any direction or specified directions). In Proceedings of the 2003 IEEE International Conference on Acoustics, Speech, and Signal Processing, Hong Kong, China, 6–10 April 2003; Volume 3, p. III-357.
15. Lorenzo-Ginori, J.V. An approach to the 2D hilbert transform for image processing applications. In Proceedings of the International Conference Image Analysis and Recognition, Montreal, QC, Canada, 22–24 August 2007; Springer: Berlin/Heidelberg, Germany, 2007; pp. 157–165.
16. Sharma, M.K.; Joseph, J.; Senthilkumaran, P. Selective edge enhancement using anisotropic vortex filter. *Appl. Opt.* **2011**, *50*, 5279–5286. [CrossRef] [PubMed]
17. Han, Y.J.; Guo, C.S.; Rong, Z.Y.; Chen, L.M. Radial Hilbert transform with the spatially variable half-wave plate. *Opt. Lett.* **2013**, *38*, 5169–5171. [CrossRef] [PubMed]
18. Sharma, M.K.; Joseph, J.; Senthilkumaran, P. Directional edge enhancement using superposed vortex filter. *Opt. Laser Technol.* **2014**, *57*, 230–235. [CrossRef]
19. Wang, Y.; Fang, J.; Zheng, T.; Liang, Y.; Hao, Q.; Wu, E.; Yan, M.; Huang, K.; Zeng, H. Mid-infrared single-photon edge enhanced imaging based on nonlinear vortex filtering. *Laser Photonics Rev.* **2021**, *15*, 2100189. [CrossRef]
20. Gozali, R.; Nguyen, T.A.; Bendau, E.; Alfano, R.R. Compact OAM microscope for edge enhancement of biomedical and object samples. *Rev. Sci. Instrum.* **2017**, *88*, 093701. [CrossRef] [PubMed]
21. Liu, S.K.; Li, Y.H.; Liu, S.L.; Zhou, Z.Y.; Li, Y.; Yang, C.; Guo, G.C.; Shi, B.S. Real-time quantum edge enhanced imaging. *Optics Express* **2020**, *28*, 35415–35426. [CrossRef] [PubMed]
22. Huo, P.; Zhang, C.; Zhu, W.; Liu, M.; Zhang, S.; Zhang, S.; Chen, L.; Lezec, H.J.; Agrawal, A.; Lu, Y.; et al. Photonic spin-multiplexing metasurface for switchable spiral phase contrast imaging. *Nano Lett.* **2020**, *20*, 2791–2798. [CrossRef] [PubMed]
23. Xu, D.; Zhang, W. Implementing the edge enhancement with vortex filter in both linear and nonlinear optics. *Front. Phys.* **2023**, *11*, 1276830. [CrossRef]
24. Morales, Y.; Diaz, L.; Torres, C.; Mattos, L. Edge Detection of Fingerprint with the Radial Hilbert Transform. In Proceedings of the Latin America Optics and Photonics, Sao Sebastiao, Brazil, 10–13 November 2012; p. LM3B-3.
25. Chen, J.; Cui, X.X.; Xiao, J.; Yang, Z.H.; Liu, T.T. Properties of Image Edge Enhancement Using Radial Hilbert Transform. *Guangzi Xuebao/Acta Photonica Sin.* **2011**, *40*, 483–486. [CrossRef]
26. Jelly, R.; Patton, E.L.; Lennard, C.; Lewis, S.W.; Lim, K.F. The detection of latent fingermarks on porous surfaces using amino acid sensitive reagents: A review. *Anal. Chim. Acta* **2009**, *652*, 128–142. [CrossRef] [PubMed]

Disclaimer/Publisher's Note: The statements, opinions and data contained in all publications are solely those of the individual author(s) and contributor(s) and not of MDPI and/or the editor(s). MDPI and/or the editor(s) disclaim responsibility for any injury to people or property resulting from any ideas, methods, instructions or products referred to in the content.